International Journal of Adhesion and Adhesives 84 (2018) 257–264

Contents lists available at ScienceDirect

International Journal of Adhesion and Adhesives

journal homepage: www.elsevier.com/locate/ijadhadh

Correlation of optically stimulated electron emission with failure mode of adhesively bonded epoxy composites

Rodolfo Ledesma[a,*], William Yost[b], Frank Palmieri[b], Daniel Cataldo[c], John Connell[b]

[a] Department of Electrical and Computer Engineering, University of Virginia, Charlottesville, VA 22904, USA
[b] NASA Langley Research Center, Hampton, VA 23681, USA
[c] NASA Internships, Fellowships & Scholarships (NIFS) Program, NASA Langley Research Center, Hampton, VA 23681, USA

ARTICLE INFO

Keywords:
Photoemission
Surface characterization
PDMS
Contamination
DCB

ABSTRACT

Carbon fiber reinforced polymers (CFRP) reduce weight in aerospace and automotive applications while maintaining or improving structural performance. Additional performance gains can be realized with composites if adhesive bonding is used in place of mechanical fasteners for structural assemblies. Surface preparation for adhesive bonding plays a critical role in the assembly process. Effective techniques for monitoring the pre-bonding surface conditions are crucial to obtain surfaces free from bond-degrading contaminants, e.g. mold release agents, which are widely used in CFRP manufacturing. In this work, optically stimulated electron emission (OSEE) was used prior to and after laser ablation to measure deposited levels of polydimethylsiloxane (PDMS) on CFRP (Torayca P2302-19). OSEE was also used to model the contamination layer thickness. After the specimens were adhesively bonded with a modified epoxy film adhesive (Loctite EA 9696 Aero), they were subjected to double cantilever beam (DCB) tests to investigate the hypothesis that surface contamination species and levels affect the fracture characteristics of adhesively bonded joints. This study relates OSEE photocurrent and the classification of the bond failure modes to their PDMS surface contamination levels prior to adhesive bonding. DCB test results show that (1) the region under the traces within the load and unloading boundaries consistently correlates with the bond strength and the probability of different failure modes, and (2) bond performance at fracture depends on the surface PDMS film thickness coating prior to laser surface treatment. The decrement in bond performance in this study correlates to the OSEE readings of contaminant levels on the adherent surfaces.

1. Introduction

A successful bond between adjacent structural components must fulfill the service requirements established by the manufacturer for any given structure. Typically, these requirements include the ability to transfer loads across bonded regions under operating conditions during the useful lifetime. Operating conditions include exposure to environmental conditions (specifically large temperature and humidity changes and extreme weather conditions) as well as, for example, fuel spills or leakage of hydraulic and other fluids onto bond regions.

Success in establishing a bond between two surfaces depends on the conditions of the surfaces involved in the adhesive bonding process. Important components in the study of bonding are the cleanliness and chemical activation of the surface. The contaminant species and their respective concentrations are potential variables in determining bond quality. In this study, the following areas were examined: (1) surface cleanliness and techniques to measure surface concentrations of specific contaminants, and (2) surface ablation to remove contamination and to provide a chemically active surface to improve adhesive bonding.

Laser ablation, as a method to prepare the surface prior to adhesive bonding, is under investigation [1–3]. In previous work [2–5], it has been shown that by adjusting the laser parameters, it is possible to selectively remove the surface contamination without damaging the underlying carbon fibers or producing interlaminar damage. Under certain conditions, laser surface ablation can generate roughness, which can improve bond performance by enabling mechanical interlocking. This surface treatment provides opportunity for automation and reproducibility in the surface preparation process.

Optically stimulated electron emission (OSEE) is a photoemission based technique designed for inspection of surface cleanliness [6–10]. Consistent with an absorption process that follows the Beer-Lambert law, contamination and adherents on surfaces change the photoelectron emission from the photoemitting target surface. Reactions between a surface and contaminants cause an alteration of the surface electron

* Corresponding author.
E-mail address: ril2yn@virginia.edu (R. Ledesma).

https://doi.org/10.1016/j.ijadhadh.2018.04.003
Accepted 29 March 2018
Available online 12 April 2018

work function, which affects the efficiency of electron emission from the surface. Therefore, surface cleanliness affects photoemission based currents.

This paper presents the capabilities of OSEE as a surface quality monitoring technique for CFRP by establishing a relationship between bond failure and OSEE readings of the surface contamination level. Each specimen set was contaminated with a measured surface concentration of polydimethylsiloxane (PDMS), a major component of silicone based mold release agents, and then ablated. Silicones, even at low concentrations, are known to cause problems with adhesive bonding on CFRP surfaces [11,12]. Pre- and post-laser-ablation CFRP surfaces were examined with OSEE and other techniques. Mechanical testing, consistent with ASTM D5528-13 [12,13], was performed by applying tensile load to the adhesively bonded CFRP specimens to determine failure modes, as per ASTM D5573-99 [14].

The sensitivity and accuracy of OSEE in distinguishing unfavorable CFRP surface conditions were also investigated. A separate set of specimens, cut from eight-ply CFRP and designed to fit the OSEE instrument measurement chamber, was used to establish the sensitivity of the OSEE measurement system to PDMS levels used in the DCB specimens. The failure modes in the DCB study were correlated to the results obtained with the OSEE technique. The effects of laser parameters on the OSEE signal response were analyzed when CFRP surfaces were laser treated using different scan speeds and average laser power levels.

2. Photoemission

2.1. Optical absorption by surface contamination

In the OSEE technique, ultraviolet (UV) source radiation impinges on the target surface with a photon energy $E = h\nu$, where h is Planck's constant, and ν the incident photon frequency. When a contamination film covers the top of a target surface, the incident intensity I_0 from the UV light source travels through the contamination layer. The incident intensity undergoes photon absorption and scattering in the contamination layer. For a contamination film thickness that extends from $x = 0$ to $x = l$, the transmitted intensity I_t at $x = l$ that excites the surface is less than the incident intensity I_0 at $x = 0$. As the UV radiation passes through the contamination layer, it produces a decrease in the incident intensity I_0. The incident intensity I_0 is proportional to the photocurrent i_0 detected by OSEE. This is true when no contamination is present. However, when there is a contamination film on the target surface, the transmitted intensity I_t, after passing through the contaminant and striking the target surface, is proportional to the photocurrent i_t. If the absorption coefficient of the contaminant is $\alpha(\lambda)$, which depends on the wavelength λ, and the thickness is l, the decrease in the photocurrent owing to an absorbing medium is described by

$$i_t = i_0 e^{-\alpha(\lambda) l} \tag{1}$$

Solving for l gives

$$l = \frac{1}{\alpha(\lambda)} \ln\left(\frac{i_0}{i_t}\right) \tag{2}$$

By applying Eq. (2), contamination thickness can be determined from optically stimulated photoemission data on Si wafers used as witness surfaces to monitor contaminant exposure on CFRP.

2.2. Work function dynamics

The impingement of the UV photons on the target surface affects the photoelectron emission from that surface. If a photon is not absorbed by the contaminant layer, it will strike the target substrate surface, and cause the emission of an electron according to the Einstein equation,

$$E_{\max} = h\nu - \phi \tag{3}$$

where $E_{\max}$ is the maximum kinetic energy of an electron emitted from the surface, and ϕ is the work function of the contaminated target surface. Photoelectron generation occurs when the incident energy is greater than the threshold energy of the surface. In addition, the difference between the source photon energy and the contamination-altered work function of the target surface affects the efficiency of the electron emission [15].

3. Experimental

3.1. Materials

The methods for the composite fabrication and the sample preparation have been previously described [3,12]. For the OSEE experiments, unidirectional CFRP panels (30.5 cm × 30.5 cm, 1.85 mm thick) were fabricated from eight plies of unidirectional Torayca P2302-19 (T800H/3900-2) prepreg. The curing process was performed in an autoclave at 177 °C for 2 hours under 690 kPa (6.9 atm). Release from the caul plate was achieved using Airtech A4000V release film, a fluorinated ethylene propylene (FEP) film, which was placed between the caul plate and the prepreg plies. Tool and caul surfaces were pre-treated with Zyvax WaterShield, a silicone-based mold release agent dispersed in water. The vacuum bagging setup and its constituents for the fabrication of unidirectional CFRP panels are shown in Fig. 1. The laminates used for OSEE measurements were cut with a water jet into square specimens of 3.81 cm × 3.81 cm. For the fracture toughness test, 10-ply CFRP panels (30.5 cm × 30.5 cm, 2.08 mm thick) were prepared with the same procedure and machined by a water jet along the carbon fiber direction to produce samples of 2.5 cm × 24.1 cm.

3.2. Sample contamination

Composite surfaces, except for the control surface, were contaminated prior to laser ablation. Contamination on CFRP samples was produced by spraying PDMS diluted with hexanes to various concentrations, leading to different layer thicknesses. Using witness silicon wafers (Si[100], 10.2 cm diameter), low (~10 nm) and medium (~60 nm) contamination levels were measured by using variable angle spectroscopic ellipsometry (VASE) [16–18] with a J.A. Woollam VB-400 control module and HS-190 scanning monochromator. Data were collected in the wavelength range from 370 nm to 900 nm with a 10 nm step size at different incident angles: 65°, 70°, and 75°. Using witness aluminum coupons, the film thickness of high contamination levels (~1 μm) was determined by weight difference using an analytical balance with a nominal resolution of 0.01 mg. Both methods, VASE and weight difference, were used to infer the thickness of PDMS on CFRP.

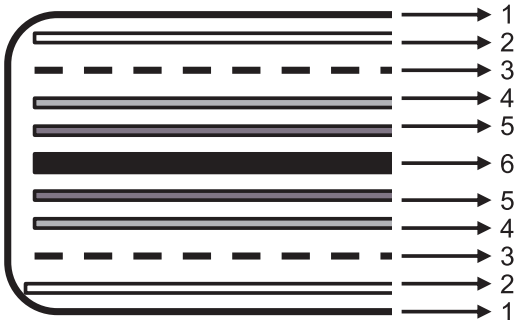

Fig. 1. Vacuum bagging setup for the fabrication of unidirectional CFRP panels (both the eight-ply, used for OSEE data, and the 10-ply, used for fracture testing): 1. Low temperature bag material, 2. Breather fabric, Airtech Airweave N10, 3. Porous release layer, Airtech Release Ease 234 TFP, 4. Stainless steel caul plate, 5. FEP release film, Airtech A4000V, and 6. Plies of prepreg, Torayca P2302-19.

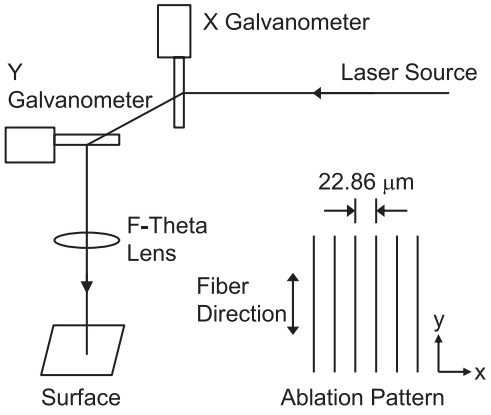

Fig. 2. A galvanometer-based optical scanner and a laser source. The ablation pattern on the surface was produced along the fiber direction with a line pitch of 22.86 μm. The coordinate frame shows the direction of fibers and the ablation pattern.

3.3. Laser ablation

Fig. 2 shows the galvanometer-based optical scanner controlled laser system for ablation of CFRP samples. The galvanometer scanning unit controls the laser beam deflection along both X and Y axes. The stationary laser beam was guided to the surface by the galvanometer scanners, and focused by an f-theta lens, which provides a flat image field on the plane of interest.

During ablation, the CFRP sample was held stationary while the galvanometer unit scanned the surface. The Coherent AVIA Nd:YAG laser system used for laser ablation was operated at 355 nm wavelength (3.5 eV photon energy). The pulse frequency was set to 80 kHz. The measured pulse width was 35 ns (FWHM). The average laser power was measured with a thermopile sensor (3A-SH) and a Nova II laser power meter from Ophir-Spiricon.

CFRP specimens were laser ablated with parallel lines, which were produced in the fiber orientation at 22.86 μm line pitch and 25.4 cm/s scan speed. The average radiant fluence F, defined as the energy irradiated on the surface per unit area, is calculated by

$$F = \frac{P_{\text{avg}}}{v_{\text{scan}} d_{\text{pitch}}} = \frac{E_p f}{v_{\text{scan}} d_{\text{pitch}}} \tag{4}$$

where P_{avg} is the average laser power, E_p the laser pulse energy, f the laser pulse frequency, v_{scan} the scan speed, and d_{pitch} the line pitch.

3.4. Spectroscopy

One set of control CFRP surfaces was characterized for surface elemental components by X-ray photoelectron spectroscopy (XPS) before and after laser surface treatment. The XPS analysis was performed on a Surface Science Instruments SSX-100 spectrometer with a monochromatic Al K-alpha X-ray (1.486 keV photon energy) source. The analysis area was 800 μm × 800 μm.

Another set of CFRP samples (control and contaminated) was inspected after laser surface ablation to verify the presence of Si by energy-dispersive X-ray spectroscopy (EDS). The EDS analysis was conducted with an Oxford Instruments X-Max 50 mm^2 microanalysis system attached to a Hitachi scanning electron microscope (SEM). The acceleration voltage during the analysis was 5 kV.

3.5. Optically stimulated electron emission

The OSEE apparatus used in this study was a prototype unit specifically designed for surface contamination research [19]. This OSEE unit applies a constant electric field for the electron collection process and a fixed UV light intensity source, which actively controls the intensity of the 185 nm line of the mercury spectrum. The regulation of photon flux and electric field tightly control the photoemission process for accurate contamination assessment during CFRP surface inspection.

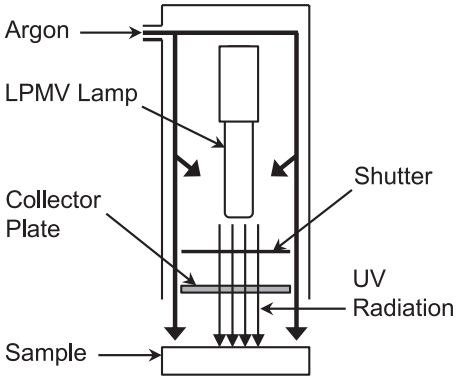

Fig. 3. Diagram of the OSEE sensor and the target sample. The LPMV lamp chamber and the test area are purged with argon. The collector bias voltage is 200 V.

The diagram of the OSEE inspection probe head [19] for CFRP surface inspection is shown in Fig. 3. A low-pressure mercury vapor (LPMV) lamp illuminated the surface under inspection with a measured photon flux of 49×10^{12} photons/s/cm^2. The photoelectrons emitted from the CFRP surface were drawn by the collector plate (a fused silica plate with the collector electrode coated onto the surface toward the specimen), which was positively biased at 200 V. The circular test area had a diameter of 2.54 cm. The distance from the collector to the target surface was 5.72 mm. The LPMV chamber was maintained in an argon environment. For each measurement, the test environment (the region between the collector plate and the specimen) was also purged with argon.

Two of the mercury lines that most contribute to the electron emission are 185 nm (6.7 eV photon energy) and 254 nm (4.9 eV photon energy). Photoemission studies, from previous tests on steel substrates, showed that the 185 nm emission line was typically responsible for 95% of the OSEE signal [7].

3.6. Adhesive bonding

Within 48 hours of laser ablation, pairs of CFRP panels were bonded with the modified epoxy film adhesive Loctite EA 9696 Aero and cured for 1 hour in an autoclave at 121 °C under 680 kPa (6.8 atm). A 7.62 cm long, 12.5 μm thick film of FEP was included in the layup to create a precrack. Using a modification of ASTM D5528-13 [12,13], samples were machined with a water jet into five specimens (2.5 cm × 24.1 cm) with notched ends for mounting directly on a clevis grip.

3.7. Double cantilever beam testing

The double cantilever beam (DCB) test method was used to mechanically test the bonded CFRP structures. With this method, the ends of a DCB specimen, as shown in Fig. 4, are pulled apart causing crack propagation along the adhesive bond line and crack opening displacement parallel to the load direction. The bonded specimen included an initial crack a_0 of ~70 mm; the exerted load P gradually opens the adhesively bonded specimen as the crack propagates.

3.8. Failure mode analysis

Of the six potential failure modes described in ASTM D5573-99 [14], only the four presented in Fig. 5 were observed in this study. Failure mode analysis was performed with the image processing and analysis software ImageJ [12,20].

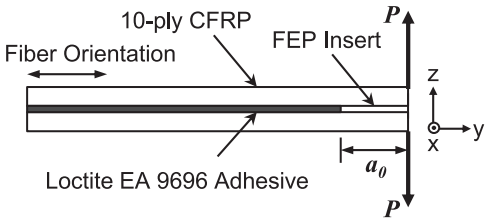

Fig. 4. Diagram of a DCB specimen. The coordinate frame is aligned with that shown in Fig. 2. The x-direction is out of the paper. The z-direction is the direction of the applied load *P*, while the y-direction is along the fiber orientation direction.

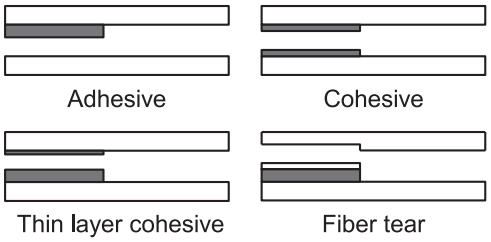

Fig. 5. Failure modes for adhesively bonded fiber-reinforced polymers, showing the schematic diagrams of the various failure modes encountered in this study, according to ASTM D5573-99.

4. Results and discussion

4.1. Laser ablation

In Fig. 6, the ablation depth and width are shown as a function of the average laser power. The difference between ablation depth and width for the same average power was caused by the way in which power was absorbed around the focal point when striking the surface; more energy was channeled into width ablation than into depth ablation. Since the energy profile of the laser beam was essentially Gaussian, the surface ablation is nonuniform. Logarithm functions relating ablation depth with average laser power were fit to the depth and width data. From the logarithm formulae, the depth is y_d and the width y_w. From the width fitting equation, the ablation threshold is ~ 53 mW.

4.2. OSEE response characteristics

Fig. 7 shows the characteristic regions of the OSEE photoemission response, and the time-domain progression of the measured photocurrent from a CFRP surface under test. Once the current reaches its maximum, it decreases monotonically. The value of the OSEE response

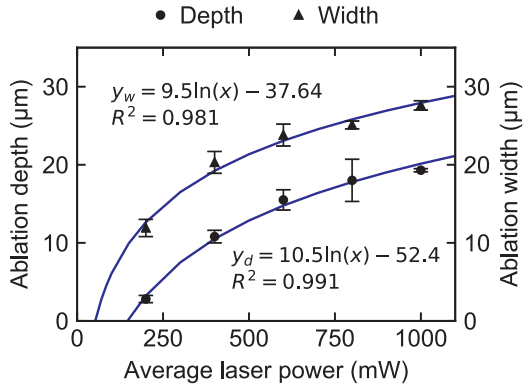

Fig. 6. Ablation width and depth values as functions of the average laser power. The solid lines are the logarithmic fitting functions. The width fitting curve intersects the ablation threshold at ~53 mW.

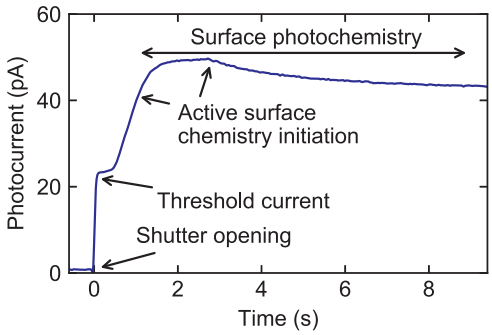

Fig. 7. Characteristic regions of OSEE response for a CFRP sample. After the shutter opens completely, the initial photocurrent is stable for ~ 400 ms. From the threshold value, the current rises rapidly to a maximum point. After that, the current decreases monotonically.

was recorded at ~150 ms after the shutter of the OSEE instrument opened completely and the OSEE response stabilized. The OSEE photocurrent at this point was the threshold current, I_{th}, which was the value recorded before photo-activated chemical processes commenced.

4.3. PDMS optical absorption properties

Eq. (1) was used to calculate the effective absorption coefficient of PDMS on the p-type silicon wafer from the plot shown in Fig. 8. To exclude the effects of roughness and heterogeneity associated with CFRP surfaces, a p-type Si[100] wafer substrate was used to evaluate the absorption coefficient of PDMS on the OSEE photocurrent response. The photocurrent measurement for a Si[100] substrate was then based on the OSEE instrument's photocurrent readings under the same conditions used to measure photocurrents on the CFRP specimens. Under these conditions, the effective absorption coefficient of PDMS was $0.25 \pm 0.04\ \mathrm{nm}^{-1}$.

4.4. Photoemission from laser ablated CFRP surfaces

Table 1 shows the surface characterization data, obtained by XPS, of control CFRP samples before and after laser ablation. The presence of silicone was detected by using the Si 2p peak that was located around the binding energy of 102.3 eV. After laser ablation, there was a decrease in the atomic percentage of Si from 3.4 to 1.2. This means that the silicone from the CFRP manufacturing was partly removed.

Fig. 9 summarizes the OSEE measurements for the CFRP coupons before and after laser ablation for different PDMS thicknesses. The average laser power chosen for the ablation process was 800 mW. The control sample was an untreated CFRP. The PDMS contaminated samples yielded low OSEE responses. The high absorption by PDMS at 185 nm [21] was thought to be the contributing factor. The absence of

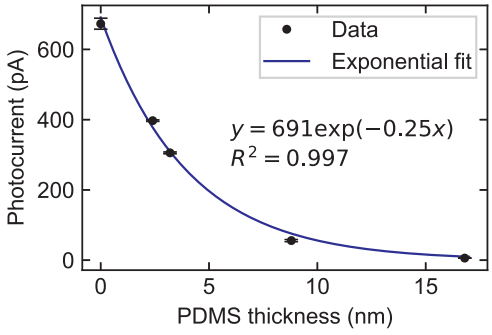

Fig. 8. Photoemission response from p-type Si[100] substrate contaminated with PDMS. The exponential fit is in agreement with Eq. (1). The effective absorption coefficient is $0.25 \pm 0.04\ \mathrm{nm}^{-1}$.

Table 1
XPS atomic percentage (at.%) for control CFRP surfaces before and after laser ablation.

Element	Atomic percentage (at.%)	
	Before laser ablation	After laser ablation
C 1s	46.4 ± 0.3	78.1 ± 0.8
F 1s	33.3 ± 0.6	0.4 ± 0.1
O 1s	13.9 ± 0.5	12.9 ± 0.8
Si 2p	3.4 ± 0.2	1.2 ± 0
N 1s	2.4 ± 0.3	6.1 ± 0.4
S 2p	0.7 ± 0	1.4 ± 0.2

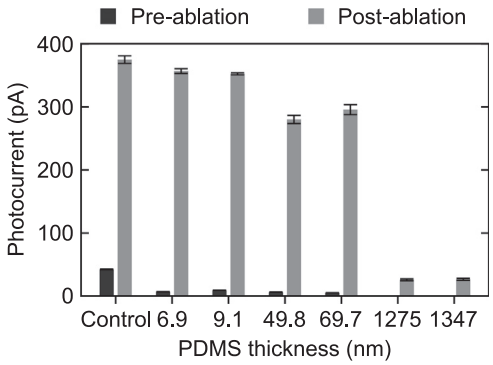

Fig. 9. OSEE photocurrent measured at I_{th} for different PDMS thicknesses on CFRP surfaces.

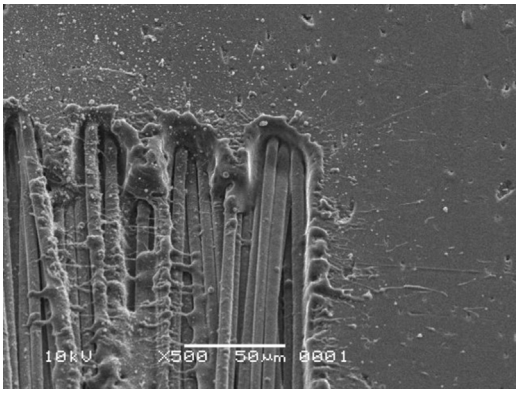

Fig. 10. SEM micrograph of a CFRP surface laser ablated at 800 mW average power. Unbroken fibers are exposed underneath the resin surface layer.

electron emissivity of PDMS at 6.7 eV was well established and was not a factor, since PDMS has a photoelectron emission threshold of ~8.4 eV [22]. After the laser ablation treatment, the OSEE current increased significantly, which indicates a large change in the surface emission. Using the previously mentioned parameters for laser treatment, the resin surface layer in the CFRP structure was removed, and unbroken fibers were exposed, as shown in Fig. 10. Therefore, both resin and contamination layers were laser ablated simultaneously. The exposure of carbon fibers can lead to fiber tear failure mode [12,23]. Previous work has demonstrated that improved bond performance (~100% cohesive failure mode) has been achieved with minimal or negligible fiber exposure [23]. Since the carbon fibers are more electrically conductive and photoresponsive than the matrix resin [24], the exposure of the fibers favored higher OSEE response. Thus, the untreated and contaminated CFRP surfaces were differentiated from the laser ablated surfaces by the OSEE measurements. However, the CFRP samples that were contaminated with high PDMS levels of approximately 1 µm (1275 nm and 1347 nm) still yielded low OSEE current, owing to the

Table 2
EDS atomic percentage (at.%) of CFRP samples with remaining PDMS after laser ablation.

PDMS thickness (nm)	Atomic percentage (at.%) after laser ablation				
	C	O	N	S	Si
Control	84.71 ± 0.8	8.25 ± 0.5	5.68 ± 0.5	1.37 ± 0.06	0
6.9	84.98 ± 0.7	8.33 ± 0.007	5.59 ± 0.8	1.12 ± 0.2	0
9.1	85.07 ± 0.4	8.16 ± 0.6	5.77 ± 0.2	1.01 ± 0.04	0
49.8	86.37 ± 0.01	7.37 ± 0.4	4.81 ± 0.3	1.45 ± 0.15	0
69.7	85.84 ± 0.3	8.08 ± 0.14	5.03 ± 0.1	1.05 ± 0.1	0
1275	78.63 ± 0.44	11.59 ± 0.15	3.76 ± 0.1	0.79 ± 0.02	5.24 ± 0.7
1347	75.74 ± 3.2	12.24 ± 1.7	3.62 ± 0.7	0.75 ± 0.13	7.67 ± 2.4

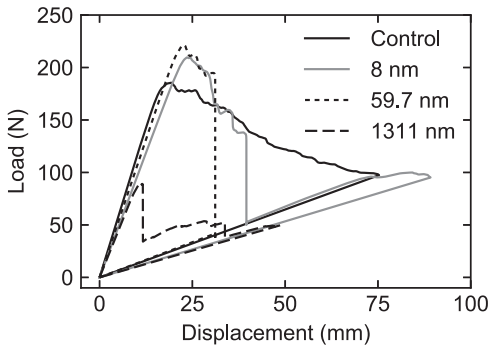

Fig. 11. Load versus displacement traces for select DCB specimens. The CFRP adherends were contaminated with PDMS coatings and laser treated prior to adhesive bonding.

incomplete removal of the PDMS layer. This was verified by EDS as shown in Table 2.

4.5. Mechanical testing and failure mode analysis

Fig. 11 shows the load-displacement traces after mechanical testing for select CFRP specimens, which are representative of their data set. The load-displacement traces were plotted for specimens with similar crack extensions of 7.89 ± 0.07 cm. As indicated by the curvature near the onset of failure (Fig. 11), the DCB specimens did not undergo linear elastic fracture. The high toughness of the epoxy film adhesive (Loctite EA 9696 Aero) contributed to the nonlinear fracture behavior as more ductility was introduced. In addition, the bonded structures were comprised of nonlinear elastic materials, with polymeric interfaces and composite bulk substrates. Thus, linear-elastic fracture mechanics (LEFM) methods could not be applied reliably to calculate the fracture toughness. Instead, a qualitative comparison of the regions under the traces within the load and unloading boundaries indicates decreasing bond performance with increasing PDMS thickness on the CFRP surfaces prior to laser ablation and bonding. As the crack propagated along the bond line, various failure modes were observed.

Fig. 12 shows the photocurrent obtained after laser surface treatment, and before adhesive bonding, plotted against the cohesive failure mode calculated from the DCB tests. A higher value of photocurrent signifies that bonding is improved between the adhesive and the adherends. This is likely due to the removal of more contaminant and a consequent increase in available surface area for bonding. The OSEE photocurrent increased as contaminant levels decreased, and the target surface was chemically activated after laser ablation, as shown in Fig. 9. The data suggest a relationship between the cohesive failure mode of the fracture surfaces and the OSEE photocurrent from target surfaces prior to adhesive bonding.

The failure modes depicted in Fig. 5 were assessed by visual inspection and image analysis software. Fig. 13 shows the surfaces of the failure modes obtained by using the image software ImageJ. Each

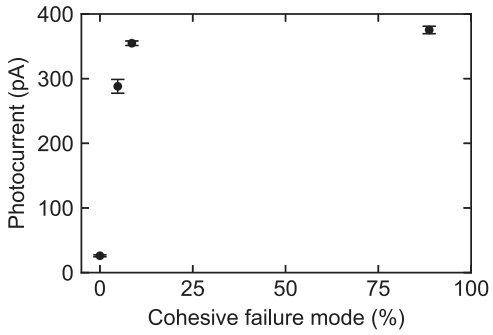

Fig. 12. Photocurrent versus cohesive failure mode. The failure modes were analyzed after DCB testing using ImageJ and confirmed by visual inspection.

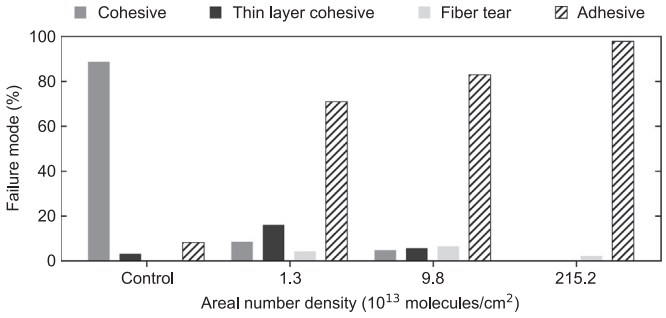

Fig. 14. Failure modes determined after DCB testing versus the PDMS areal number density. The CFRP surfaces were contaminated with different PDMS areal number densities and laser treated prior to bonding.

image was constructed by folding the top beam about the fiber orientation axis, and placing it edge-to-edge with the bottom beam. The center line in each image denotes the edge-to-edge placement. In this alignment, the top and bottom fracture surfaces are both visible. The contoured character of the fracture surface shows up in opposite relief on opposite sides of the center line. Fig. 13a shows a specimen that presented adhesive failure due to contamination residue, causing a poor bond between the adhesive and specimen surface. When the surface is properly treated, the bond between the adhesive and the specimen surface is stronger than the adhesive bond line. Thus, the fracture surface undergoes cohesive failure, as shown in Fig. 13b. Fig. 13c shows the results of a thin layer cohesive failure, in which thick adhesive layers were present on one substrate surface, and thin layers on the other. When the top fiber layer of the CFRP substrate fails, delamination occurs, as shown in Fig. 13d. Fiber tear failures may occur from a variety of possible surface treatment techniques, such as sanding, grit blasting, and laser treatment, as well as crack propagation dynamics. Depending on the ablation energy, the laser treatment process may expose some carbon fibers in the top ply, to which the adhesive would directly bond, as shown in Fig. 10.

Fig. 14 displays the percentages of failure modes from the DCB tests as a function of the PDMS molecular areal number density, which was deposited before laser ablation. The CFRP surfaces were laser treated with 800 mW average power prior to the adhesive bonding. Five bonded joints were mechanically tested for each surface condition. The results reveal more clearly the effects of the silicone-based contamination, even after laser ablation, by showing predominantly high percentage of adhesive failure. Large differences in failure modes were reported between the control surface, and those with low PDMS levels. As shown in Fig. 9, the OSEE photocurrent of the control CFRP was slightly higher than that of the low PDMS areal number densities. The uncontaminated control sample produced cohesive failure of ~89%, in contrast to the low percentage of cohesive failure (< 10%) for the contaminated samples prior to laser ablation. The poor bonding performance in previously contaminated surfaces was also observed, even after the laser ablation process was applied. The poor performance may imply that PDMS and similar compounds remained on the surface, because they have low absorption for wavelengths above 200 nm [21]. This may affect their removal by laser ablation at 355 nm, although the mechanisms that discourage removal are not entirely clear. Since this is an ongoing work, laser ablation conditions for removing PDMS (~25 nm thick) from CFRP surfaces have been determined. Higher OSEE photocurrents indicate higher probability of cohesive failure over adhesive failure, since larger photocurrent implies less density of surface contamination.

Table 3 summarizes the results of measurements from photoemission (pre-ablation and post-ablation) against contaminant film thickness. The PDMS film thickness was varied by adjusting the concentration of PDMS in the solvent, which was thermally treated to completely evaporate remaining hexanes from the surface prior to the photocurrent measurements. The three levels of PDMS contaminants were chosen to provide guidance for future investigations into effects of contaminant levels on adhesive bond strength in CFRP-based structures.

4.6. CFRP surface topography

Laser parameters used for treatment of CFRP surfaces not only change the surface chemistry but also the surface morphology. Different laser powers created variations in selective patterns and topographical modifications on the surface prior to bonding. The parameters analyzed in this study were the average laser power and the scan speed. The average laser power exposures were 100 mW, 300 mW, and 800 mW, which have been previously used for laser surface treatment [2,16].

To check the effects of delayed measurements on CFRP material after exposure, control CFRP samples were tested within 24 hours of laser ablation and again after 1 week. The target samples were stored for 1 week in a desiccator with air at room temperature, normal atmospheric pressure, and at 21.8 ± 5.8 % relative humidity. Fig. 15 shows the effect of different laser power levels on the OSEE photocurrent. Fig. 16 shows the OSEE photocurrent for surfaces that were laser ablated at 800 mW at three different scan speeds (25.4 cm/s, 50.8 cm/s, and 101.6 cm/s). For the measurements taken within 24 hours, the photocurrent was similar for the three different laser average powers. After 1 week, there was a decrease in the photocurrent. This decrement in photocurrent may have been caused by surface contamination by organic or inorganic compounds from the air, oxidation

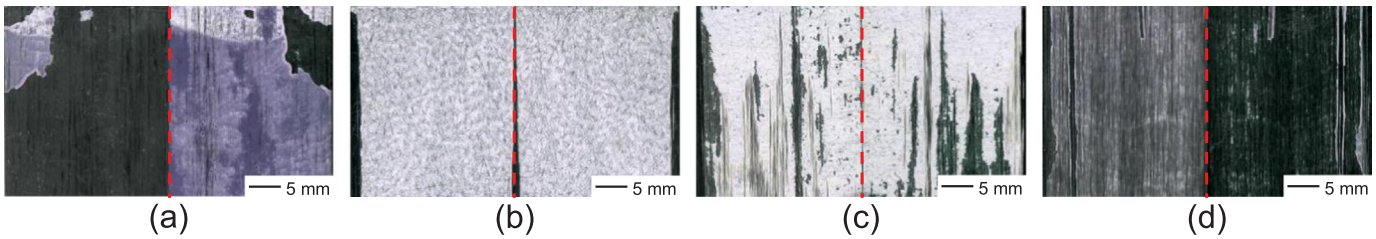

Fig. 13. DCB failure surfaces, placed edge-to-edge, (top on the left; bottom on the right, as shown by the center line) for CFRP with predominantly (a) adhesive, (b) cohesive, (c) thin layer cohesive, and (d) fiber tear modes.

Table 3
Relationship between PDMS thickness and photocurrent I_{th}.

Areal number density (10^{13} molecules/cm^2)	Film thickness (nm)	Film areal density (μg/cm^2)	Pre-ablation I_{th} (pA)	Post-ablation I_{th} (pA)
Control	0	0	42.3 ± 0.4	375.3 ± 5.7
1.3	8 ± 1.6	0.77 ± 0.15	8 ± 1.3	354.8 ± 3.5
9.8	59.7 ± 14.1	5.8 ± 1.4	5.7 ± 0.6	288.1 ± 10.7
215.2	1311 ± 51	126.5 ± 5	–	26.2 ± 1.5

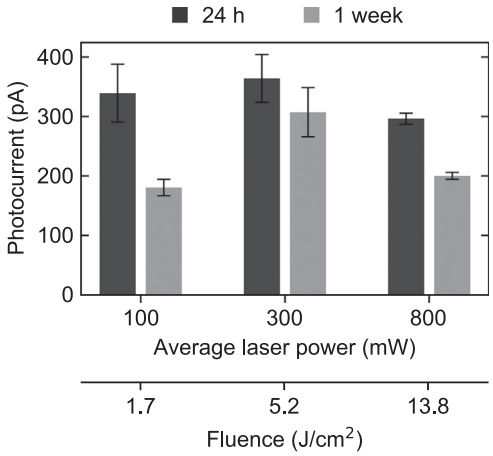

Fig. 15. OSEE readings for CFRP samples laser ablated at different laser power levels within 24 hours and again after 1 week.

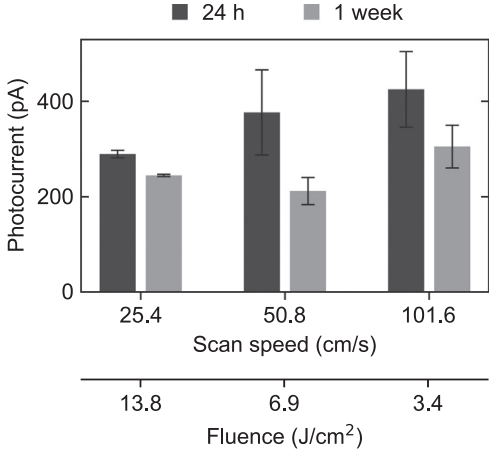

Fig. 16. OSEE readings for CFRP samples laser ablated at 800 mW at different scan speeds within 24 hours and again after 1 week.

growth on the surface, and passivation of active chemical species initially formed.

The particles adsorbed on the surface were held by weak physical bonds, in comparison to chemical bonds. These particles can alter the OSEE photocurrent measured. The London-van der Waals equation describes the adhesion force between a spherical particle and a flat surface,

$$F_{LW} = \frac{Ar}{6d^2} \tag{5}$$

where A is the Hamaker coefficient, which depends on the particle and surface composition, r the radius of a spherical particle, and d the distance of separation. Theoretically, the oxidation of the surface is produced by adsorption of oxygen on the surface that bonds with the valence electrons of the surface, and thus produces carbonyl, hydroxyl, and epoxide functional groups. The oxidation films on the surface affect

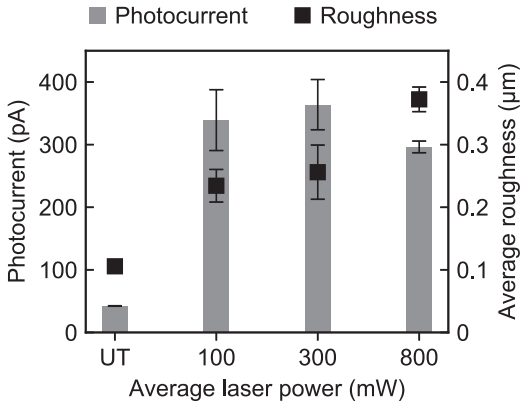

Fig. 17. Relationship between OSEE photocurrent and average roughness as a function of the average laser power. The untreated (UT) CFRP is compared with laser ablated CFRP surfaces. The bar graph represents the photocurrent (left ordinate), while the solid squares represents the average roughness (right ordinate).

the work function of the material. The oxidation of species on the CFRP surface is nonuniform due to the roughness and heterogeneity of the laser ablated composite material. For the CFRP surfaces freshly laser ablated, the surface becomes rougher as the radiant fluence increases. As surfaces become rougher, both the UV light scattering on the surface and the increase in electron emission angle affect the photoelectron emission [6].

The CFRP surface topography was analyzed with a FRT MicroProf optical profilometer. The average roughness was determined with the phase correct filter according to ISO 11562 [25]. Fig. 17 depicts the relationship between the OSEE photocurrent and the average roughness for different CFRP surface conditions after laser ablation. As the roughness increases, the photocurrent increases to a certain level, followed by a photoemission decrease at 13.8 J/cm^2 (800 mW). This change in the surface morphology affects the photocurrent. Possible mechanisms for this photocurrent emission change may include the increase in exposed surface due to the increase in surface roughness, and surface chemistry initiated by the UV exposure from the OSEE apparatus. Kinetics of photoelectrons may also play a role in the photocurrent variations. Despite this, photocurrent differences due to contamination level within each category were observed. However, ablation exposure in photocurrent interpretation to deduce contaminant level must be considered.

5. Conclusions

In this study, OSEE provided a very sensitive technique that was clearly able to detect small amounts of silicone surface contamination, even mono-molecular layer segments partially covering a surface. OSEE photocurrent measurements gave an effective absorption coefficient for a PDMS contamination layer, as confirmed by measurements with known contamination thicknesses on a Si[100] substrate. Furthermore, with OSEE measurements, it was possible to identify whether and to what degree a CFRP surface was laser ablated. The data suggest that increases in OSEE photocurrent with increasing ablation are owing to

the exposed carbon fibers near the surface. For the material system studied, the qualitative analysis of the regions under the traces within the load and unloading boundaries correlated with the pre-bond OSEE photocurrent intensities. This correlation indicates that the OSEE technique may be used to predict bond performance. It was clear that OSEE photocurrent levels were also affected by surface roughness, however effects of surface roughness on bonding were not investigated when surface contamination was also a factor. Based on this study, it may be possible to predict bond performance by measuring the contaminant concentration on adherent surfaces prior to applying the adhesive.

Acknowledgments

This work was supported by the NASA (No. NNL09AA00A) Advanced Composites Project. The authors thank Dr. James Ratcliffe for helpful discussions. The authors also thank the following personnel from NASA Langley Research Center: Daniel Perey and Joshua Brown for OSEE data collection and insightful discussions, John Hopkins for conducting the laser surface treatment, and Hoa Luong, Sean Britton, and Michael Oliver for laminate fabrication, bonded specimen fabrication, and specimen preparation.

References

[1] Wohl C, Belcher M, Connell J, Hopkins J. Modification of surface energy via direct laser ablative surface patterning. US Patent 8987632 (2015).
[2] Palmieri F, Hopkins J, Wohl C, Lin Y, Connell J, Belcher M, Blohowiak K. Laser surface preparation of epoxy composites for secondary bonding: optimization of ablation depth. SAMPE Baltimore, 2015.
[3] Palmieri F, Belcher M, Wohl C, Blohowiak K, Connell J. Laser ablation surface preparation for adhesive bonding of carbon fiber reinforced epoxy composites. Int J Adhes Adhes 2016;68:95–101.
[4] Fischer F, Kreling S, Jäschke P, Frauenhofer M, Kracht D, Dilger K. Laser surface pretreatment of CFRP for adhesive bonding in consideration of the absorption behaviour. J Adhes 2012;88:350–63.
[5] Fischer F, Kreling S, Dilger K. Surface structuring of CFRP by using modern excimer laser sources. Phys Procedia 2012;39:154–60.
[6] Gause R. A noncontacting scanning photoelectron emission technique for bonding surface cleanliness inspection. In: Proceedings of the 5th Annual NASA NDE Workshop, 1987.
[7] Welch C, Abedin M, Yost W. Optically stimulated electron emission: current-voltage response and spectral sensitivity. In: Thompson D, Chimenti D, editors. Review of Progress in Quantitative Nondestructive Evaluation. New York: Plenum Press; 1992. p. 2155–62.
[8] Brune K, Lima L, Noeske M, Thiel K, Tornow C, Dieckhoff S, Hoffmann M, Stübing D. Pre-bond quality assurance of CFRP surfaces using optically stimulated electron emission. In: Proceedings of the 3rd International Conference Engineering Against Failure, 2013, pp. 300–307.
[9] Brune K, Tornow C, Noeske M, Wiesner T, Barbosa AQ, Stamboroski S, et al. Surface analytical approaches contributing to quality assurance during manufacture of functional interfaces. Appl Adhes Sci 2015;3.
[10] Tornow C, Schlag M, Lima L, Stübing D, Hoffman M, Noeske P-L, et al. Quality assurance concepts for adhesive bonding of composite aircraft structure - characterisation of adherent surfaces by extended NDT. J Adhes Sci Technol 2015;29:2281–94.
[11] Markatos D, Tserpes K, Rau E, Brune K, Pantelakis S. Degradation of mode-I fracture toughness of CFRP bonded joints due to release agent and moisture pre-bond contamination. J Adhes 2014;90:156–73.
[12] Palmieri F, Ledesma R, Fulton T, Arthur A, Eldridge K, Thibeault S, Lin Y, Wohl C, Connell J. Picosecond pulsed laser ablation for the surface preparation of epoxy composites. SAMPE Seattle, 2017.
[13] ASTM D5528-13, Standard test method for mode I interlaminar fracture toughness of unidirectional fiber-reinforced polymer matrix composites. ASTM International (2013).
[14] ASTM D5573-99, Standard practice for classifying failure modes in fiber-reinforced-plastic (FRP) joints. ASTM International (2012).
[15] Maurer R. Handbook of physics. In: Condon E, Odishaw H, editors. Photoelectric effect. McGraw-Hill; 1967.
[16] Palmieri F, Ledesma R, Cataldo D, Lin Y, Wohl C, Gupta M, et al. Controlled contamination of epoxy composites with PDMS and removal by laser ablation. SAMPE Long Beach; 2016.
[17] Woollam J, Snyder P, Rost M. Variable angle spectroscopic ellipsometry: a nondestructive characterization technique for ultrathin and multilayer materials. Thin Solid Films 1988;166:317–23.
[18] Woollam J, Snyder P. Fundamentals and applications of variable angle spectroscopic ellipsometry. Mater Sci Eng B 1990;5:279–83.
[19] Perey D. A portable surface contamination monitor based on the principle of optically stimulated electron emission (OSEE). JANNAF Propulsion and Joint Subcommittee Meeting, 1996.
[20] Rasband W. Image J, ⟨http://imagej.nih.gov/ij/⟩(1997–2016).
[21] Graubner V-M, Jordan R, Nuyken O, Lippert T, Hauer M, Schnyder B, et al. Incubation and ablation behavior of poly(dimethylsiloxane) for 266 nm irradiation. Appl Surf Sci 2002;197–198:786–90.
[22] Koizumi H, Lacmann K, Schmidt W. Light-induced electron emission from silicone oils. J Phys D: Appl Phys 1992;25:857–61.
[23] Ledesma R, Palmieri F, Dennie J, Dowdell J, Fitz-Gerald J, Connell J. Detection of trace silicone contamination on CFRP surfaces by picosecond LIBS. The Adhesion Society, 2018.
[24] Chekanov Y, Ohnogi R, Asai S, Sumita M. Electrical properties of epoxy resin filled with carbon fibers. J Mater Sci 1999;34:5589–92.
[25] DIN EN ISO 11562, Geometrical Product Specifications - Surface texture: Profile method - Metrological characteristics of phase correct filters. International Organization for Standardization (1998).